Mechanism of the $^{16}O(^7Li,\alpha)^{19}F$ reaction at 20 MeV

S. Mordechai* and H. T. Fortune
Physics Department, University of Pennsylvania, Philadelphia, Pennsylvania 19104
(Received 18 June 1984)

The $^{16}O(^7Li,\alpha)^{19}F$ reaction has been investigated at an incident energy of 20 MeV. Complete angular distributions were measured in the angular range $\theta_{lab}=7.5°-157.5°$ using a multiangle spectrograph. Known $(sd)^3$ states are populated about twice as strongly as the core-excited four-particle—one-hole (4p-1h) states. Angular distributions for members of the ground-state band show only a moderate forward-angle rise, and those of the negative-parity band and other weak states are approximately symmetric around 90°. Results have been analyzed in terms of Hauser-Feshbach compound-nucleus calculations and finite-range distorted-wave Born approximation calculations in which the three transferred nucleons enter the *sd* and/or $1p$ shells. The contribution of the compound-nucleus cross section has been estimated. The data for the $K^\pi=\frac{1}{2}^+$ and $K^\pi=\frac{1}{2}^-$ bands in ^{19}F could be well fitted by an incoherent sum of direct and compound reaction cross sections. Simple analysis of the integrated cross sections based on a $(2J+1)$ rule is consistent with results of the Hauser-Feshbach calculations. Comparison between the present experimental results and previous triton cluster transfer reactions on ^{16}O emphasizes the enhanced compound/direct ratio for the 4p-1h and other weak states in the present data.

I. INTRODUCTION

Considerable effort has been spent in recent years to understand the reaction mechanism responsible for the population of states by the $(^7Li,\alpha)$ reaction[1–4] and other multinucleon Li-induced transfer reactions, i.e., $(^7Li,X)$ (Refs. 5–7) and $(^6Li,X)$ (Refs. 8 and 9), where $X=$p, d, t, ^{3}He, or α. Early studies of the $(^7Li,\alpha)$ reaction at bombarding energies above 30 MeV found a very high degree of selectivity in populating final states.[1–4] In the $^{16}O(^7Li,\alpha)^{19}F$ reaction at 35 MeV,[3] strong population of the low-lying $(sd)^3$ states in ^{19}F was observed, as would be expected if the reaction proceeds via a direct three-nucleon transfer to a doubly-closed-shell ^{16}O nucleus. In such a mechanism the low-lying negative-parity 4p-1h states in ^{19}F would be only weakly excited through the 2p-2h and 4p-4h components in the ^{16}O g.s. wave function. However, no detailed direct-reaction analysis was performed in Ref. 3.

At lower energies, compound-nucleus formation might be expected to compete with direct processes—especially for the weaker states. Thus, the compound component could be best estimated from transitions to negative-parity 4p-1h states or to other core-excited states.

In the present work, we report the results of a study of the $^{16}O(^7Li,\alpha)^{19}F$ reaction at an energy of 20 MeV. This study was undertaken to attempt to determine the compound and direct reaction components of the reaction. Our choice of the target was motivated by the approximate closed-shell nature of ^{16}O(g.s.) and the large number of low-lying final states in ^{19}F (Ref. 10) which have known J^π. For most states below an excitation energy of about 5.5 MeV the dominant configuration has also been determined. These include the $K^\pi=\frac{1}{2}^+$ g.s. band which has a predominant $(sd)^3$ structure, the negative parity $K^\pi=\frac{1}{2}^-$ band which has an $(sd)^4(1p_{1/2})^{-1}$ character, and higher core-excited states, e.g., $(sd)^5(1p)^{-2}$, $(sd)^6(1p)^{-3}$, etc.

II. EXPERIMENTAL PROCEDURE

The experiment was performed with a 20-MeV ^{7}Li beam from the University of Pennsylvania Tandem Accelerator. The oxygen gas was enriched to 99.5% and contained in a gas cell with no entrance window. Gas pressure was 15.0 Torr. Outgoing alpha particles exited the gas cell through a window and were momentum

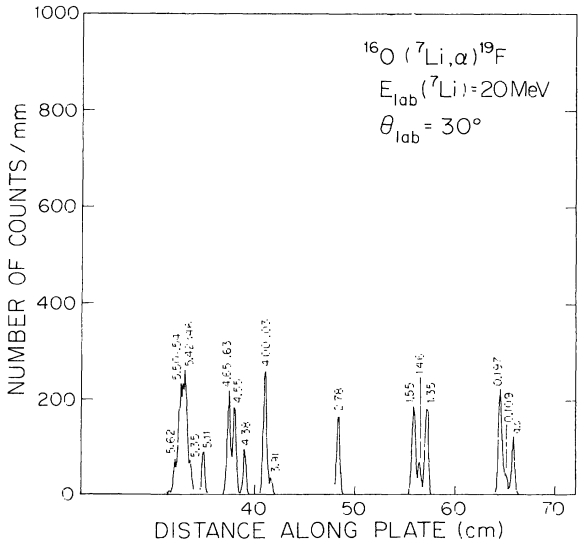

FIG. 1. Alpha spectrum from the $^{16}O(^7Li,\alpha)^{19}F$ reaction measured at 20 MeV incident energy and at a laboratory angle of 30°. The levels in ^{19}F are indicated by their excitation energies.

analyzed with a multiangle spectrograph and recorded on Ilford K-1 nuclear emulsion plates in the angular range of 7.5°—157.5° in 7.5° steps. The exposure was 5500 μC. Mylar foil absorbers of variable thickness (0—0.5 mm) were placed in front of the focal plane to stop all ions with $z > 2$.

Displayed in Fig. 1 is a spectrum measured at 30° covering an excitation energy range of about 5.6 MeV. States are indicated by their excitation energies. The energy resolution was about 30 keV full width at half maximum (FWHM) and arose primarily from energy loss of the ^{7}Li ions in the target and straggling of the α particles in the exit window. Absolute cross sections were obtained from the measured gas pressure and integrated beam current. The uncertainty in the overall cross-section scale is estimated at 20%.

III. RESULTS

Angular distributions were extracted for all observed states in ^{19}F up to an excitation energy of 5.46 MeV.

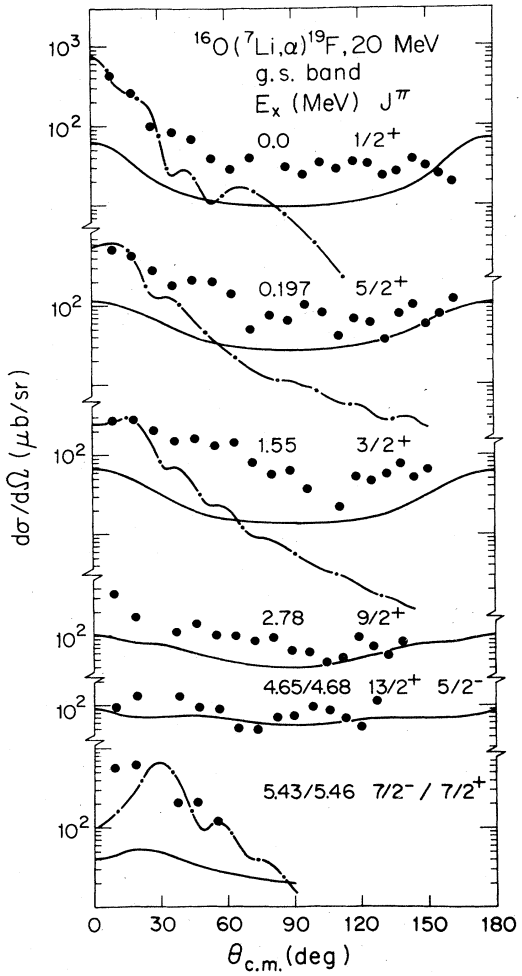

FIG. 2. Angular distributions for the g.s. band in ^{19}F measured in the $^{16}O(^7Li,\alpha)^{19}F$ reaction at 20 MeV. The curves are the results of a finite-range DWBA calculation (dashed-dotted) and statistical model calculation (solid) using the code STATIS normalized by a factor of 0.5 (see the text).

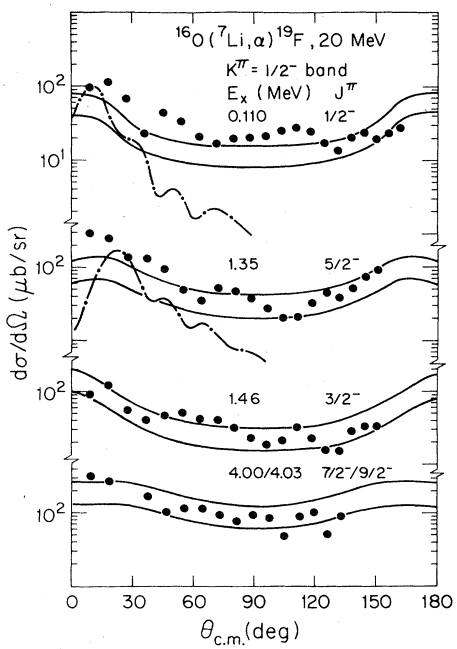

FIG. 3. Same as Fig. 2 but for the $K^\pi = \frac{1}{2}^-$ band in ^{19}F. The two Hauser-Feshbach curves (solid) have been calculated using the code STATIS and normalized by factors of 1.0 and 0.5, respectively.

They are presented in Figs. 2—4 and compared with results of finite-range distorted-wave Born approximation (FRDWBA) calculations using the code DWUCK5 (Ref. 11) and with results of Hauser-Feshbach statistical

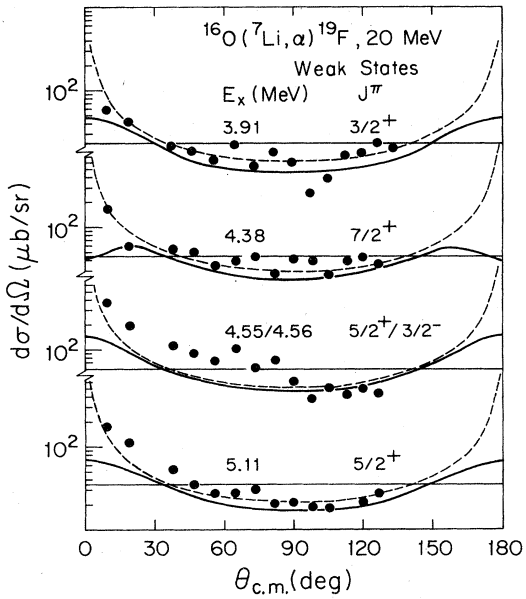

FIG. 4. Angular distributions for the weak states observed in the $^{16}O(^7Li,\alpha)^{19}F$ reaction at 20 MeV up to 5.46 MeV excitation. The dashed curves and the straight solid lines are $1/\sin\theta$ and $\sigma(\theta)$=const fits to the data normalized to give an integrated cross section of $36.6(2J+1)$ μb. The curved solid lines represent the HF calculations multiplied by a normalization factor of 0.5.

TABLE I. Results from the $^{16}O(^{7}Li,\alpha)^{19}F$ reaction at 20 MeV.

Present	Literature[a]			σ_{tot} (μb)[d]			$\sigma_{tot}(0°-90°)/(2J+1)$ (μb)	
E_x (keV)	E_x (keV)	J^π	K^π	0°–90°	90°–180°	$\frac{\sigma(0°-90°)}{\sigma(90°-180°)}$	$\pi=+$	$\pi=-$
0	0	$\frac{1}{2}^+$	$\frac{1}{2}^+$	443.1	191.6	2.31	221.5	
106±8	109.89	$\frac{1}{2}^-$	$\frac{1}{2}^-$	223.9	147.4	1.52		112.0
201±10	197.14	$\frac{5}{2}^+$	$\frac{1}{2}^+$	1071.8	451.9	2.37	178.6	
1351±9	1345.67	$\frac{5}{2}^-$	$\frac{1}{2}^-$	543.1	273.2	1.99		90.5
1478±13	1458.7	$\frac{3}{2}^-$	$\frac{1}{2}^-$	305.9	159.5	1.92		76.5
1566±10	1554.04	$\frac{3}{2}^+$	$\frac{1}{2}^+$	837.2	377.1	2.22	209.3	
2803±9	2779.85	$\frac{9}{2}^+$	$\frac{1}{2}^+$	728.1	419.8	1.73	72.8	
3936±11	3908.17	$\frac{3}{2}^+$	$\frac{3}{2}^+$	138.6	160.1	0.87	34.7	
4051±14	3998.7	$\frac{7}{2}^-$	$\frac{1}{2}^-$	859.1	477.2	1.80		47.7[c]
	4032.5	$\frac{9}{2}^-$	$\frac{1}{2}^-$					
4415±13	4377.7	$\frac{7}{2}^+$	b	308.4	218.2	1.41	38.6	
4586±12	4549.9	$\frac{5}{2}^+$	$\frac{3}{2}^+$	650.3	202.2	3.22	65.0[c]	65.0[c]
	4556.1	$\frac{3}{2}^-$						
4692±11	4648	$\frac{13}{2}^+$	$\frac{1}{2}^+$	534.4	588.6	0.91	38.1[e]	
	4682.5	$\frac{5}{2}^-$						
5140±11	5106.6	$\frac{5}{2}^+$		280.1	141.7	1.98	46.7	
5469±7	5418	$\frac{7}{2}^-$		1306.5			81.7[c]	81.7[c]
	5463.5	$\frac{7}{2}^+$	$\frac{1}{2}^+$					

[a]Reference 10.
[b]This level is believed to be an $(sd)^3$ state. However, in Ref. 10, it is listed as having $K^\pi=\frac{3}{2}^+$.
[c]$\sigma_{tot}(0°-90°)/\Sigma(2J+1)$.
[d]$\sigma_{tot}=2\pi\Sigma\sigma(\theta_i)\sin\theta_i\Delta\theta_i$.
[e]Assuming the total CS is predominantly due to the $\frac{13}{2}^+$ $K^\pi=\frac{1}{2}^+$ state.

compound-nucleus calculations using the code STATIS.[12] Details of these calculations will be given in a later section. Figures 2 and 3 display the data for the g.s. band and for the negative-parity ($K^\pi=\frac{1}{2}^-$) band, respectively, and Fig. 4 contains the data for all other (weakly) excited states. The data of Fig. 4 are also compared with two additional estimates of the compound-nucleus cross sections which will be discussed in Sec. IV.

Values of σ_{tot} obtained by integrating all points in the angular distributions in the ranges (0°–90°) and (90°–180°) are listed in Table I. The table also gives the ratios

$$\sigma_{tot}(0°-90°)/\sigma_{tot}(90°-180°)$$

and

$$\sigma_{tot}(0°-90°)/(2J+1)\ .$$

The integrated cross sections $\sigma_{tot}(0°-90°)$ are plotted vs $2J+1$ (where J is the final-state spin) in Fig. 5.

Simple features of the results for both the integrated and the differential cross sections indicate that no one single reaction mechanism can account for the data. The ratio

$$\sigma_{tot}(0°-90°)/\sigma_{tot}(90°-180°)$$

is not as large as would be expected for a pure direct triton cluster transfer reaction. In fact, in two cases (the transitions to the 3.908 and 4.648/4.682 MeV states) the ratio is slightly smaller than unity, indicating that the cross sections (CS's) at backward angles are somewhat

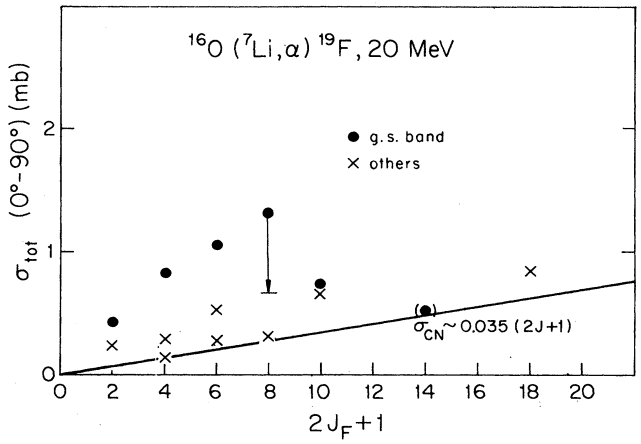

FIG. 5. Plot of $\sigma_{tot}=2\pi\int_{0°}^{90°}\sigma(\theta)\sin\theta\,d\theta$ vs $2J_F+1$ for all levels below 5.47 MeV in ^{19}F.

TABLE II. Comparison between the cross sections for the $K^\pi=\frac{1}{2}^+$ and $\frac{1}{2}^-$ states in ^{19}F measured in the $^{16}O(^7Li,\alpha)^{19}F$ reaction at 20 and 35 MeV.

^{19}F			$^{16}O(^7Li,\alpha)$ 20 MeV		$^{16}O(^7Li,\alpha)$ 35 MeV[d]	
E_x (MeV)	J^π	K^π	$(d\sigma/d\Omega)_{max}$ (μb)	Ratio[a]	$(d\sigma/d\Omega)_{max}$ (μb)	Ratio[a]
0	$\frac{1}{2}^+$	$\frac{1}{2}^+$	450	0.26	340	0.15
0.11	$\frac{1}{2}^-$	$\frac{1}{2}^-$	115		50	
0.197	$\frac{5}{2}^+$	$\frac{1}{2}^+$	538	0.57	1200	0.04
1.35	$\frac{5}{2}^-$	$\frac{1}{2}^-$	306		150	
1.55	$\frac{3}{2}^+$	$\frac{1}{2}^+$	288	0.44	870	0.09
1.46	$\frac{3}{2}^-$	$\frac{1}{2}^-$	127		80	
2.78	$\frac{9}{2}^+$	$\frac{1}{2}^+$	341	0.48[c]	1300	
4.00/4.03	$\frac{7}{2}^-,\frac{9}{2}^-$	$\frac{1}{2}^-$	330[b]	0.57[c]	480[b]	0.18[c]
5.47	$\frac{7}{2}^+$	$\frac{1}{2}^+$	291		1300	

[a] $[d\sigma/d\Omega(\pi=-)]_{max}/[d\sigma/d\Omega(\pi=+)]_{max}$.
[b] Summed cross section for the doublet 4.00/4.03.
[c] Assuming the $\frac{7}{2}^-$ and $\frac{9}{2}^-$ states share the total strength equally.
[d] Reference 3.

larger in these cases than those at forward angles. On the other hand, the values of

$$\sigma_{tot}(0°\text{—}90°)/(2J+1)$$

presented in the last column of Table I are far from being a constant as would be expected for a pure compound-nucleus (CN) mechanism under certain conditions.[13–15] The scatter in

$$\sigma_{tot}(0°\text{—}90°)/(2J+1)$$

is also indicated in Fig. 5, which shows a plot of $\sigma_{tot}(0°\text{—}90°)$ vs $2J+1$. States which belong to the g.s. band are populated more strongly than the negative-parity states with the same J. The lowest CS's in the reaction give an estimated value of 35 μb for the minimum ratio $\sigma_{tot}/(2J+1)$, which can be considered as a rough estimate of the CN cross section.

The angular distributions of the negative-parity band (Fig. 3) and of other weak states (Fig. 4) are structureless and approximately symmetric around 90° as expected for a CN mechanism, whereas those of the g.s. band (Fig. 2) show also a clear forward-angle rise typical of a direct-reaction process.

Table II presents another feature of the data by comparing the maximum differential cross sections of the $K^\pi=\frac{1}{2}^-$ and $\frac{1}{2}^+$ states measured in the present work and in the $^{16}O(^7Li,\alpha)^{19}F$ reaction at 35 MeV.[3] In a direct process of three nucleon transfer on ^{16}O the 4p-1h states can be populated only via the 2p-2h or 4p-4h component in ^{16}O g.s. The ratios

$$\sigma_{max}(J,\pi=-)/\sigma_{max}(J,\pi=+)$$

at 35 MeV range between 4% and 18%, which is close to the magnitude of the core excited component in ^{16}O g.s.,[16] while those of the present work range between 26% and 57%, indicating that the CN contribution is significantly stronger in the present work. These remarks are made more quantitative in the following.

IV. ANALYSIS AND DISCUSSION

A. Direct reaction calculations

The exact finite-range DWBA code DWUCK5 (Ref. 11) was used to perform the calculations for the direct-reaction process. In these calculations the triton cluster was bound to an alpha in a relative $2p$ state forming ^7Li. The binding potential was of the Woods-Saxon type and was adjusted to give the binding energy of 2.465 MeV. The bound-state wave functions of ^{19}F were also generated in the same type of potential with the depth adjusted to reproduce a binding energy of $(11.699-E_x)$ MeV, where E_x is the excitation energy of the final state in ^{19}F. The ^7Li optical-model parameters used in the present analysis were taken from the recent $^{6,7}Li$ optical-model parameter compilation of Cook (Ref. 17). For the exit channel a standard alpha set has been used. Table III lists the optical parameters used in the present analysis as well as those used in the reanalysis of the 35-MeV data of Ref. 3. Except for the transition to the g.s. of ^{19}F which can proceed only via $L=1$ transfer and for the transition to the 0.109-MeV $\frac{1}{2}^-$ state for which the allowed L transfers are 1 and 2, for all other excited states three L values are allowed due to the coupling with the $L=1$ $^7Li=\alpha+t$ g.s. These were added incoherently to yield the CS's shown in Figs. 2 and 3. The normalizations of the DWBA curves to the data will be discussed in a later section.

For a stripping reaction the experimental differential CS is given by

$$(d\sigma/d\Omega)_{exp}=NsS(l,J)\frac{(2J+1)}{(2J_i+1)}(d\sigma/d\Omega)_{DW5},$$

TABLE III. Optical parameters used in the analysis of the $^{16}O(^7Li,\alpha)^{19}F$ reaction. Strengths are in MeV and lengths in fm.

	$E(^7Li)$	V	r_0	a_0	W	r_I	a_I	W_D	r_D	a_D	r_c	λ
$^{16}O+^7Li$[a]	20	33.1	1.73	0.85				10.3	1.87	0.72	1.5	
$^{16}O+^7Li$[a]	35	189.5	1.21	0.74	21.3	2.00	0.82				1.3	
$^{19}F+\alpha$[b]		180.0	1.42	0.56	16.5	1.42	0.56				1.4	
$BS1(^{19}F=^{16}O+t)$		c	1.26	0.65								0.0
$BS2(^7Li=\alpha+t)$		d	1.26	0.65								0.0

[a]Reference 8.
[b]Reference 27.
[c]Adjustable to give a binding energy of 11.699 MeV $-E_x$.
[d]Adjustable to give a binding energy of 2.465 MeV.

where N is the normalization constant for the reaction and theoretically is expected to be 1 for an exact finite-range calculation. The quantity s is the spectroscopic factor of the ^{7}Li projectile and measures the probability that ^{7}Li g.s. is composed of $t+\alpha$ clusters, and $S(l,J)$ is the spectroscopic factor of the final state in ^{19}F. In this expression, $(d\sigma/d\Omega)_{DW5}$ is the incoherent sum of cross sections for the allowed L values leading to a specific final J.

B. Analysis of the integrated cross sections

The procedure described here assumes that the only important reaction mechanisms are the direct and *statistical* compound ones, and that the interference between these two mechanisms is negligible. If the $(2J+1)$ rule were to hold for the CN component of the cross section, we could express the integrated experimental CS as follows:

$$\sigma_{tot}(0°-90°)=(2J+1)\sigma_{CN}+Ns\sigma_{dir}(0°-90°)\ ,$$

where σ_{dir} is defined as

$$\sigma_{dir}(0°-90°)=S\frac{(2J+1)}{(2J_i+1)}\sigma_{DW5}(0°-90°)\ ,$$

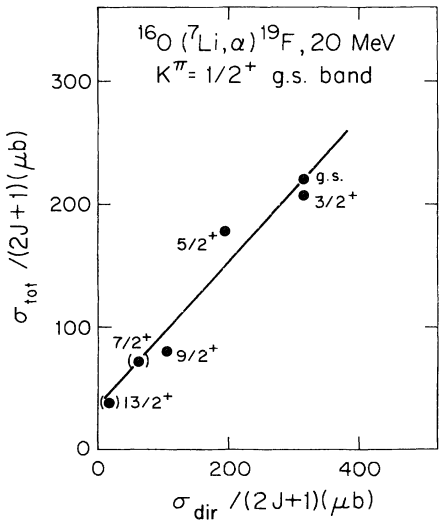

FIG. 6. Graph of $\sigma_{tot}(0°-90°)/(2J+1)$ vs $\sigma_{dir}(0°-90°)/(2J+1)$ for the g.s. band. The straight line is a least square fit to the data.

then

$$\sigma_{tot}/(2J+1)=\sigma_{CN}+Ns\sigma_{dir}/(2J+1)\ ,$$

as $J_i=0$. Thus a plot of $\sigma_{tot}/(2J+1)$ vs $\sigma_{dir}/(2J+1)$ (Fig. 6) should give a straight line with intercept and slope determining σ_{CN} and Ns, respectively. The last two columns of Table IV give the values for $\sigma_{tot}/(2J+1)$ and $\sigma_{dir}/(2J+1)$ for the g.s. band. The spectroscopic factors S included in $\sigma_{dir}/(2J+1)$ were taken from a recent shell-model calculation[23] and are also listed in the table. The line drawn in Fig. 6 was obtained from a least-squares fit to the data. The data points for the $\frac{7}{2}^+$ and $\frac{13}{2}^+$ states are marked in parentheses since they are both members of unresolved doublets, as indicated in Table IV. The $\frac{13}{2}^+$ state was not included in the fit. The results indicate that $\sigma_{CN}=36.6\pm1.0$ μb and $Ns=0.583\pm0.004$. This estimation of the CN cross sections is in excellent agreement with the value of 35 μb obtained from Fig. 5, and discussed earlier.

C. Hauser-Feshbach calculations

Calculations of the compound-nuclear cross sections were performed using the computer code STATIS.[12] The details of such calculations were outlined in Refs. 18 and 19 and the formalism was taken from Refs. 20 and 21. The nuclear level density was taken to be of the form[22]

$$\rho(U,J)=\frac{(2J+1)}{12a^{1/4}(U+t)^{5/4}(2\sigma^2)^{3/2}}\times\exp[2(aU)^{1/2}]_{exp}\left[-\frac{(J+\frac{1}{2})^2}{2\sigma^2}\right]\ ,$$

where the nuclear temperature t is obtained from $U=at^2-t$ and $\sigma^2=\mathcal{I}t/\hbar^2$. The rigid-body moment of inertia is

$$\mathcal{I}=(\tfrac{2}{5})mAR^2(1+0.31\beta+0.44\beta^2)\ \text{ for } R=r_0A^{1/3}\ ,$$

where m is the mass of a nucleon and A is the nuclear mass in u. The excitation energy is defined as $U=E-b\delta$, where b is 2 for even-even, 1 for odd-even, and zero for odd-odd nuclei, and δ is the pairing energy [taken to be 2.25 MeV, which is the average of neutron and proton pairing parameters in the (sd) shell]. No critical angular momentum cutoff was used and the calculated cross sections were normalized to the data by a factor

TABLE IV. Analysis of the $K^\pi = \frac{1}{2}^+$ g.s. rotational band.

Energy level (MeV)	J^π	$\sigma_{tot}(0°-90°)$ (μb)	σ_{DW5}[a]$(0°-90°)$ (μb)	S[b] Th	$\frac{\sigma_{tot}}{2J+1}$ (μb)	$\frac{\sigma_{dir}}{2J+1}$[c] ($\mu$b)
g.s.	$\frac{1}{2}^+$	443.1	352.15	0.90	221.6	316.9
0.197	$\frac{5}{2}^+$	1071.8	273.3	0.72	178.6	196.8
1.55	$\frac{3}{2}^+$	837.2	449.9	0.70	209.3	314.9
2.78	$\frac{9}{2}^+$	728.1	84.6	0.72	72.8	60.9
4.64	$\frac{13}{2}^+$	534.4[d]	32.5	0.60	38.1[f]	19.5
5.47	$\frac{7}{2}^+$	1306.5[e]	208.0	0.50	81.7	104.0

[a] $\sigma_{DW5} = 2\pi \sum \sigma(\theta_i)\sin\theta_i \Delta\theta_i$.

[b] Reference 23.

[c] $\sigma_{dir} = Ss\frac{2J+1}{2J_i+1}\sigma_{DW5}(0°-90°)$, thus, $\sigma_{dir}/2J+1 = S\sigma_{DW5}(0°-90°)$ assuming $s(^7Li)=1$.

[d] Summed CS for the doublet 4.65/4.68 with J^π $\frac{13}{2}^+$ and $\frac{5}{2}^-$.

[e] Summed CS for the doublet 5.42/5.47 with J^π $\frac{7}{2}^-$ and $\frac{7}{2}^+$.

[f] Assuming the total CS is predominantly due to the $\frac{13}{2}^+$ state.

which is common to all states, as will be discussed later.

The preceding equation has two unspecified parameters: the level-density parameter and the moment of inertia $\mathscr{I}$. We used the standard level-density parameter of 0.125 MeV^{-1} for the *sd* shell and $r_0 = 1.2$ fm, $\beta = 0$ in the calculation of $\mathscr{I}$.

The transmission coefficients have been calculated using the ^{7}Li optical-model parameters listed in Table III and also using the equation

$$T_l(E) = \frac{1}{1+\exp[(E_{BR}-E)/\mathrm{del}_C E_{Bl}]} ,$$

where

$$E_{Bl} = \frac{Z_1 Z_2 e^2}{R_c} + \frac{\hbar^2}{2\mu_c R_c^2}(l+\tfrac{1}{2})^2 ;$$

Z_1, Z_2, A_1, A_2 are the charges and masses of the particles;

$$R_c = R_{c0}(A_1^{1/3} + A_2^{1/3}) ;$$

$$\mu_c = m_A \frac{A_1 A_2}{A_1 + A_2}, \quad m = \text{atomic mass unit} .$$

It was found that calculated cross sections using the preceding expression for $T_l(E)$ and with $R_{c0} = 1.25$ fm and $\mathrm{del}_c = 0.06$ are close to those obtained using transmission coefficients from the optical model potential. We have thus used for simplicity the parametrized T_l's throughout the paper. The results of the Hartree-Fock (HF) calculations are shown in Figs. 2–4.

Figure 7 shows a schematic diagram of the CN formed in the collision of $^{16}O + ^7Li$ at 20 MeV and its subsequent decay to various channels. Numbers next to the arrows indicate the integrated Hauser-Feshbach CS for each channel. The total fusion CS is predicted to be 550 mb and thus the α channel exhausts only about 11% of the total CS. The single neutron is the strongest decay channel ($\sim$70% of the total CS). Except for the enhanced neutron decay, the calculated cross sections show the expected Q_{gg} dependence, namely the CS plotted against the Q value (Q_{gg}) fall on a straight line on a logarithmic scale.

In terms of σ_{HF} and σ_{dir} we express the integrated CS as an incoherent sum:

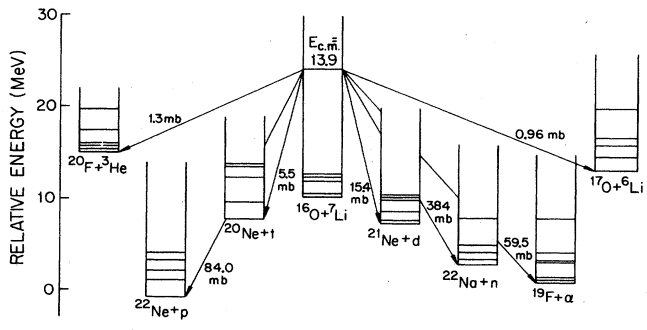

FIG. 7. Schematic diagram showing the channels taken into account in the HF calculations. Numbers next to the arrows indicate the total cross section for that decay mode.

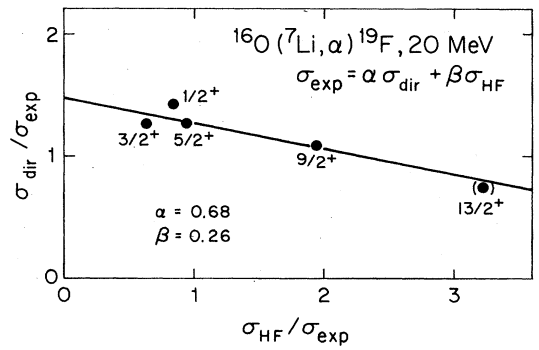

FIG. 8. Plot of $\sigma_{dir}(0°-90°)/\sigma_{exp}(0°-90°)$ vs $\sigma_{HF}(0°-90°)/\sigma_{exp}(0°-90°)$ for the g.s. band in ^{19}F. The line represents a least square linear fit to the data.

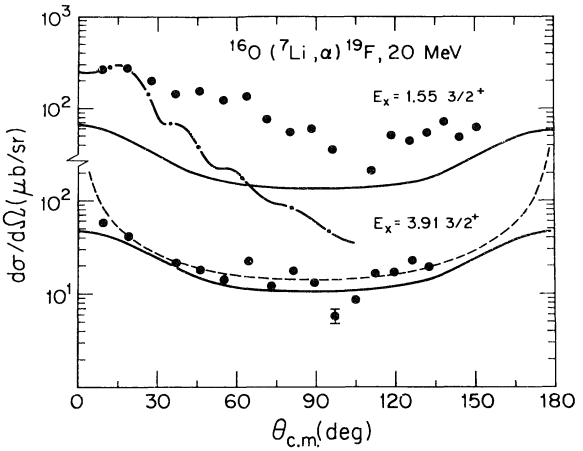

FIG. 9. Experimental angular distributions for the two $\frac{3}{2}^+$ states at 1.55 and 3.91 MeV populated in the ^{16}O(^{7}Li,α)^{19}F reaction at 20 MeV. The dashed-dotted and the solid curves are the results of FRDWBA and statistical model calculations, accordingly. The dashed line shown with the 3.91-MeV data is a $1/\sin\theta$ fit.

$$\sigma_{\text{exp}}=\alpha\sigma_{\text{dir}}+\beta\sigma_{\text{HF}} .$$

Where $\sigma_{\text{dir}}=S(2J+1)\sigma_{\text{DWS}}$ as was defined earlier, σ_{HF} is the calculated total Hauser-Feshbach cross section, and α and β are normalization factors to be determined experimentally,

$$\sigma_{\text{dir}}/\sigma_{\text{exp}}=1/\alpha-(\beta/\alpha)(\sigma_{\text{HF}}/\sigma_{\text{exp}}) .$$

Figure 8 shows a plot of $\sigma_{\text{dir}}/\sigma_{\text{exp}}$ vs $\sigma_{\text{HF}}/\sigma_{\text{exp}}$ for the g.s. band. The data fall approximately on a straight line. A least-squares fit to the data yields $\alpha=0.68$ and $\beta=0.26$. The deduced number for α deviates only about 12% from the value of 0.58 obtained earlier. The value of β gives an overall experimental normalization factor for the calculated HF cross section.

Figure 9 shows again the angular distribution for the two lowest $\frac{3}{2}^+$ states in ^{19}F. The first at 1.55 MeV is an $(sd)^3$ state and apparently has a large direct component, whereas the second $\frac{3}{2}^+$ state at 3.91 is much weaker and its angular distribution is approximately symmetric around 90°. If we assume that the latter has no direct component then we can obtain an additional normalization for the HF calculations. The solid line in Fig. 9 is the HF calculated differential CS multiplied by a factor of 0.5. The dashed line represents another semiclassical calculation which will be described later. Thus the data for the core-excited state at 3.91 MeV indicate that a normalization factor of roughly $\frac{1}{2}$ will be required for the HF calculations rather than 0.26 as was suggested from the analysis of the integrated CS. A factor of 0.5 turns out to give a reasonably good fit for the angular distributions of other weak states shown in Fig. 4. We have thus used the same normalization factor of 0.5 for all positive-parity states populated in the present study.

The dashed and the solid straight lines shown with the data points in Fig. 4 are the results of two additional semiclassical fits to the data. The dashed line is an $\alpha'/\sin\theta$ curve where α' is a constant chosen to yield the same integrated CS as would be expected from the $2J+1$ rule for a state with spin J. If we adopt the previous value of $\sigma_{\text{CN}}=36.6$ μb then $\alpha'=36.6(2J+1)/\pi^2$. Similarly the straight line represents an isotropic distribution with a magnitude of $\sigma_J(\theta)=36.6(2J+1)/2\pi$, which also yields the same integrated cross section as would be predicted from the $(2J+1)$ rule.

D. Analysis of the g.s. band

Figure 10 presents again the angular distribution for the g.s. of ^{19}F compared with HF calculations normalized as previously indicated (dashed-dotted line), finite-range DWBA calculations (dashed line), and as their sum (solid line). The addition of the HF cross section has only a small effect at forward angles but improves the fit at the

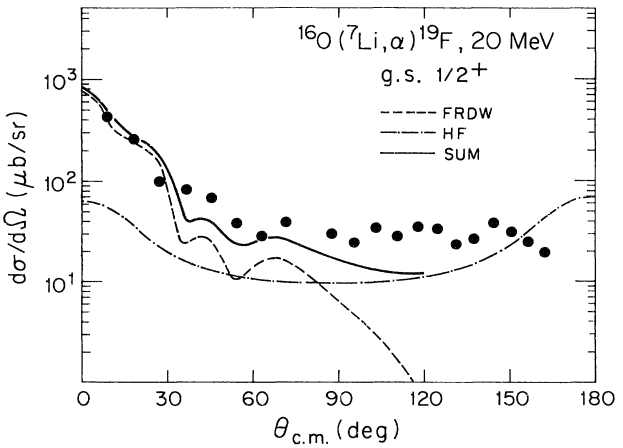

FIG. 10. Angular distribution for the g.s. of ^{19}F measured in the ^{16}O(^{7}Li,α)^{19}F reaction at 20 MeV compared with the incoherent sum (solid line) of HF calculations (dashed-dotted line) and FRDWBA calculations (dashed line).

TABLE V. Comparison between the spectroscopic factors for the g.s. band of ^{19}F measured in the present work and previous work.

Energy level (MeV)	J^π	$S(^{16}\text{O}+\text{t}\rightarrow{}^{19}\text{F})$ (^{7}Li,α)[a] 20 (MeV)	(^{6}Li,^{3}He)[b] 24 (MeV)	Th[c]
g.s.	$\frac{1}{2}^+$	0.35	0.35	0.90
0.197	$\frac{5}{2}^+$	0.40	0.38	0.73
1.55	$\frac{3}{2}^+$	0.29	0.33	0.70
2.78	$\frac{9}{2}^+$	0.39	0.32	0.72
4.64	$\frac{13}{2}^+$	0.38		0.60
5.47	$\frac{7}{2}^+$	<2.03[d]	0.27	0.50

[a]Present work,
$S=[\sigma_{\text{exp}}(\theta)-\sigma_{\text{CN}}(\theta)]/0.6(2J+1)\sigma_{\text{DWS}}(\theta)$.
[b]Reference 25.
[c]Reference 23.
[d]This upper value is set by the CS for the doublet 5.418/5.464 with $J^\pi=\frac{7}{2}^-$ and $\frac{7}{2}^+$, respectively.

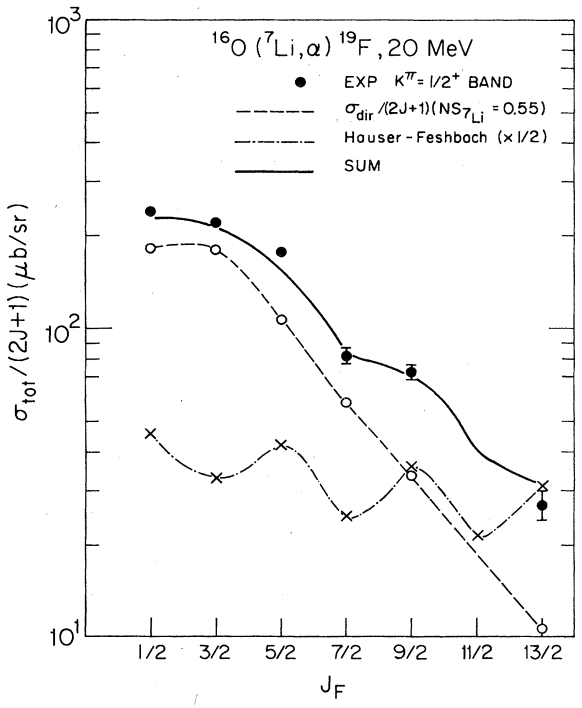

FIG. 11. Plot of $\sigma_{tot}(0°-90°)/(2J_F+1)$ vs J_F for the g.s. band. The experimental angle integrated cross sections are compared with the incoherent sum (solid line) of a direct reaction component (dashed line) and a compound nucleus component (dashed-dotted line).

backward angles. Similar behavior was observed for the other members of the g.s. band, i.e., the 0.197-MeV $\frac{5}{2}^{+}$ and the 1.55-MeV $\frac{3}{2}^{+}$ states. The $\frac{9}{2}^{+}$ and $\frac{13}{2}^{+}$ states have apparently a very small direct component due to kinematic rather than spectroscopic conditions. Since the reaction has a large Q value ($Q_{gg}=9.233$ MeV), the incoming and outgoing waves have almost the same grazing angular momentum (L grazing$=10$). This matching condition drastically reduces the direct CS amplitude for the high-spin states, although they have spectroscopic factors as large as those with lower spins (Table V).

Figure 11 presents the analysis of the integrated CS for the g.s. band in terms of direct and compound-reaction components. The dashed-dotted line represents, vs J, the integrated HF cross section after dividing by $2J+1$. The theoretical curve oscillates between 30 and 50 μb showing an odd-even effect because of the staggering of the excitation energies in the g.s. band. The direct component $\sigma_{dir}/(2J+1)$ (dashed line) shows a sharp decrease with J due to the kinematical conditions discussed earlier. The sum (solid line) accounts reasonably well for the strong J dependent integrated CS observed experimentally. The figure also indicates that for the low-spin members ($J^{\pi}=\frac{1}{2}^{+}, \frac{3}{2}^{+}, \frac{5}{2}^{+}$) the CN cross section contributes only about 20% of σ_{tot}, but this reaction process becomes significantly more dominant for the higher spin members of the g.s. band.

Estimates of the spectroscopic factors for the $K^{\pi}=\frac{1}{2}^{+}$ band may be determined experimentally after subtracting the CN component and comparing with DWUCK5 calculations. Table V presents such an analysis. The spectroscopic factors listed in the table were obtained using the relation

$$S=[\sigma_{exp}(\theta)-\sigma_{CN}(\theta)]/0.6(2J+1)\sigma_{DW5}(\theta)\ ,$$

where $\sigma_{CN}(\theta)$ is the (normalized) calculated HF cross section. The deduced spectroscopic factors are compared with the spectroscopic factors obtained from the $^{16}O(^{6}Li,^{3}He)^{19}F$ reaction at 24 MeV (Ref. 24) and with a recent shell-model calculation.[23] There is remarkable agreement between the present results and those of Ref. 24, but the theory predicts spectroscopic factors too large by a factor of about 2 in comparison with the experimental values. Of course, the S values of Ref. 24 are not absolute, as they result from a zero-range calculation. For the 5.47-MeV $\frac{7}{2}^{+}$ state only an upper limit on S could be obtained from the present study since the state could not be resolved from the 5.418-MeV $\frac{7}{2}^{-}$ state.

E. Analysis of the negative-parity band

The negative-parity band in ^{19}F with a predominant 4p-1h structure is expected to be weakly populated by a direct process in the $^{16}O(^{7}Li,\alpha)^{19}F$ reaction. The comparison between the maximum CS of states with the same

TABLE VI. Analysis of the $K^{\pi}=\frac{1}{2}^{-}$ band in ^{19}F.

E_x (MeV)	J^{π}	$\sigma_{tot}(0°-90°)/(2J+1)$ (μb)	NS[a]	$\sigma_{DW5}(0°-90°)$[b] (μb)	$N\sigma_{dir}/(2J+1)$[c] (μb)	$\sigma_{HF}/(2J+1)$[d] (μb)
0.109	$\frac{1}{2}^{-}$	111.9	0.043	325.4	14.0	72.2
1.345	$\frac{5}{2}^{-}$	90.5	0.180	119.8	21.6	66.8
1.458	$\frac{3}{2}^{-}$	76.5	0.024	414.3	9.9	77.9
3.998	$\frac{7}{2}^{-}$	47.7	0.060	235.4	14.1	60.4
4.032	$\frac{9}{2}^{-}$					

[a]Extracted in the present work from the $^{16}O(^{7}Li,\alpha)^{19}F$ data at 35 MeV (Ref. 3).
[b]$\sigma_{DW5}(0°-90°)=2\pi\sum_{\theta=0°}^{90°}\sigma(\theta_i)\sin\theta_i\Delta\theta_i$.
[c]$\sigma_{dir}/(2J+1)=S\sigma_{DW5}(0°-90°)$.
[d]Results of Hauser-Feshbach calculations. See the text.

spin but belonging to the $K^\pi = \frac{1}{2}^+$ and $\frac{1}{2}^-$ bands presented in Table II has already indicated that these latter states are populated predominantly by a CN process. Additional evidence comes from their angular distributions (Fig. 3) which are mostly symmetric around 90° for the $\frac{3}{2}^-$ and $\frac{7}{2}^-/\frac{9}{2}^-$ members. Those for the $\frac{1}{2}^-$ and $\frac{5}{2}^-$ states contain also a small forward rise that may be due to a small direct triton transfer component.

Since no spectroscopic factors could be obtained from the literature for these states, no accurate estimates of the relative sizes of the compound and direct components could be made. In order to further investigate this point we have extracted the spectroscopic factors for these states from previously published data on the $^{16}O(^7Li,\alpha)^{19}F$ reaction at 35 MeV,[3] where a direct mechanism probably dominates. The FRDWBA calculations at 35 MeV were done using the parameters listed in Table III. Table VI summarizes this analysis. The third column presents the experimental integrated CS divided by $2J+1$. The fourth column lists the values of NS obtained from our analysis of the 35-MeV data of Ref. 3. We have used these values of NS to calculate $N\sigma_{dir}/(2J+1)$ at 20 MeV, as listed in the sixth column of the table. The last column presents $\sigma_{HF}/(2J+1)$ from the STATIS calculations.

The results indicate that compound-nuclear processes contribute most (70—90%) of the reaction cross section for these core-excited states. A fit to the data requires an average normalization factor of 0.95 for the HF calculation for the negative-parity states. Therefore in Fig. 3 we have shown the data for the $K^\pi = \frac{1}{2}^-$ band together with two HF curves normalized by a factor of 0.5 (which has been suggested for the positive-parity states) and 1.0 (obtained from the analysis of the $K^\pi = \frac{1}{2}^-$ band). The data fall mainly between these two curves as would be expected.

V. COMPARISON WITH PREVIOUS RESULTS AND CONCLUSIONS

Figure 12 presents a comparison between the present results and those obtained from (a) the $^{16}O(^6Li,^3He)^{19}F$ reaction at 24 MeV,[25] (b) the $^{16}O(^7Li,\alpha)^{19}F$ reaction at 35 MeV (Ref. 3), and (c) the $^{16}O(\alpha,p)^{19}F$ reaction at 40 MeV.[26] The figure displays the ratio of the maximum cross section vs J (final-state spin). Except for Q-value effects the (α,p) and $(^6Li,^3He)$ reactions should be equivalent to the $(^7Li,\alpha)$ reaction since all three are triton transfer reactions. However, two striking facts emerge: (i) The cross-section ratio decreases significantly with increasing spin of the final state. This effect is probably due to the large differences in the Q values for the three reactions. The present reaction has $Q=9.233$ MeV, while $^{16}O(^6Li,^3He)^{19}F$ and $^{16}O(\alpha,p)^{19}F$ have $Q=4.094$ and -8.114 MeV, respectively. Therefore the last two have large angular momentum mismatch, giving a relatively enhanced population of final states with high spins, whereas the almost perfect matching conditions in the present reaction favor low L transfers. (ii) The cross section ratios for the $K^\pi = \frac{1}{2}^-$ band and other weak states are always larger than those obtained for the g.s. band. These states are populated very weakly in the predominantly direct triton cluster transfer on ^{16}O via the (α,p) $(^6Li,^3He)$, as well as the $(^7Li,\alpha)$ reaction at 35 MeV, while in the present study they all have a sizable CN cross section.

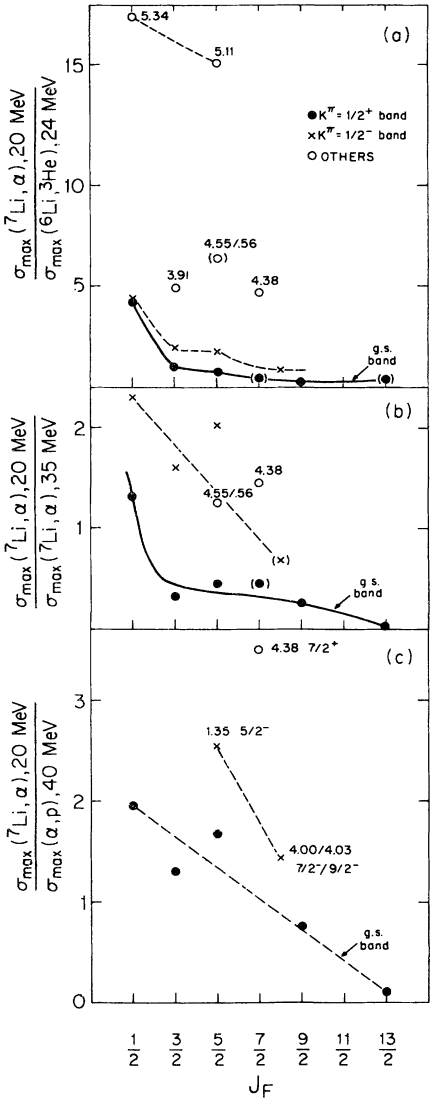

FIG. 12. Ratios of the maximum experimental cross sections measured in the present work and in the previously reported (α,p), $(^6Li,^3He)$, and $(^7Li,\alpha)$ reactions on ^{16}O vs J_F.

In conclusion, the study of the $^{16}O(^7Li,\alpha)^{19}F$ reaction has revealed that no one single reaction mechanism can account for the data at 20 MeV. An analysis in terms of an incoherent sum of direct plus compound components can reasonably well account for the measured cross sections of both positive- and negative-parity states.

An analysis of the compound-nucleus component using the $2J+1$ rule yields results which are consistent with

the statistical compound-nucleus calculations. Comparison with previous studies of ^{19}F in direct triton cluster transfer reactions emphasizes the presence of the compound component in the reaction mechanism, and gives support to our separation of the two reaction components.

ACKNOWLEDGMENTS

We are grateful to Les Bland and Richard Eckman for help in the data analysis. This work was supported by the National Science Foundation.

*Permanent address: Department of Physics, Ben-Gurion University of the Negev, Beer-Sheva, Israel.

[1]A. F. Zeller, K. W. Kemper, T. R. Ophel, and A. Johnston, Nucl. Phys. **A344**, 307 (1980).

[2]L. H. Harwood and K. W. Kemper, Phys. Rev. C **14**, 368 (1976).

[3]I. Tserruya, B. Rosner, and K. Bethge, Nucl. Phys. **A235**, 75 (1974).

[4]I. Tserruya, B. Rosner, and K. Bethge, Nucl. Phys. **A213**, 22 (1973).

[5]L. C. Dennis, A. Roy, A. D. Frawley, and K. W. Kemper, Nucl. Phys. **A359**, 455 (1981).

[6]H. T. Fortune and J. N. Bishop, Nucl. Phys. **A304**, 221 (1978).

[7]H. T. Fortune, L. R. Medsker, and J. N. Bishop, Nucl. Phys. **A309**, 221 (1978).

[8]J. Cook, L. C. Dennis, K. W. Kemper, T. R. Ophel, A. F. Zeller, C. F. Maguire, and Z. Kui, Nucl. Phys. **A415**, 114 (1984).

[9]K. M. Abdo, L. C. Dennis, A. D. Frawley, and K. W. Kemper, Nucl. Phys. **A377**, 281 (1982).

[10]F. Ajzenberg-Selove, Nucl. Phys. **A392**, 1 (1983).

[11]P D. Kunz, code DWUCK5 (unpublished).

[12]R. Stokstad, code STATIS, private communication.

[13]O. Hansen, E. Koltay, N. Lund, and B. S. Madsen, Nucl. Phys. **51**, 307 (1964).

[14]N. Macdonald, Nucl. Phys. **33**, 110 (1962).

[15]J. R. Powers, H. T. Fortune, and R. Middleton, Nucl. Phys. **A298**, 1 (1978).

[16]R. D. Lawson, F. J. D. Serduke, and H. T. Fortune, Phys. Rev. C **14**, 1245 (1976).

[17]J. Cook, At. Data Nucl. Data Tables **26**, No. 1, 20 (1981).

[18]L. C. Dennis, A. Roy, A. D. Frawley, and K. W. Kemper, Nucl. Phys. **A359**, 455 (1981).

[19]H. V. Klapdor, H. Reiss, and G. Rosner, Nucl. Phys. **A262**, 157 (1976).

[20]T. D. Thomas, Annu. Rev. Nucl. Sci. **18**, 343 (1968).

[21]E. Vogt, in *Advances in Nuclear Science,* edited by M. Baranger and E. Vogt (Plenum, New York, 1968), Vol. I.

[22]R. W. Shaw, Jr., J. C. Norman, R. Vandenbosch, and J. C. Bishop, Phys. Rev. **184**, 1040 (1969).

[23]B. H. Wildenthal, private communication.

[24]J. D. Garrett, H. G. Bingham, H. T. Fortune, and R. Middleton, Phys. Rev. C **5**, 682 (1972).

[25]H. G. Bingham, H. T. Fortune, J. D. Garrett, and R. Middleton, Phys. Rev. Lett. **26**, 1448 (1971).

[26]K. van der Borg, R. J. De Meijer, and A. van der Woude, Nucl. Phys. **A273**, 172 (1976).

[27]J. D. Garrett, R. Middleton, and H. T. Fortune, Phys. Rev. C **2**, 1243 (1970).